ELSEVIER

Chemical Engineering Journal 138 (2008) 416–424

Chemical Engineering Journal

www.elsevier.com/locate/cej

Study of a non-isothermal, non-isobaric consolidated reactive bed for chemisorption icemakers

R.G. Oliveira *, R.Z. Wang

Institute of Refrigeration and Cryogenics, Shanghai Jiao Tong University, 800 Dong Chuan Road, Shanghai 200240, PR China

Received 6 November 2006; received in revised form 6 June 2007; accepted 25 June 2007

Abstract

Kinetic, heat and mass transfer in a consolidated reactive bed for sorption icemakers were studied with an analogical model that was experimentally validated. The bed was made from expanded graphite impregnated with calcium chloride, and the coefficients of the model were assessed by minimizing the sum of the squared deviations between the observed and simulated data, for several operation conditions normally employed in the ice making process. The average error in calculated global conversion during the synthesis phase ranged from 0.012 to 0.041, depending on the experimental conditions. The average error for the simulated temperature was smaller than 1.3 °C, and the average error for the pressure close to the wall of the reactor was smaller than 50 mbar. Simulation results showed that a specific cooling power higher than 1250 W/kg of salt can be achieved with a bed of 10 mm thickness operating with an evaporation temperature of −15 °C and a heat sink temperature of 25 °C; however if the thickness of the bed is increased to 20 mm, the evaporation temperature should be at least −10 °C to produce similar results.
© 2007 Elsevier B.V. All rights reserved.

Keywords: Sorption; Modelling; Calcium chloride; Ammonia; Refrigeration

1. Introduction

Sorption heat pump and refrigeration machines are heat-powered systems that can aid the reduction of CO_2 emissions into the atmosphere when they are driven by waste heat or solar energy. Furthermore, these machines are ozone friendly because they normally employ natural refrigerants without ODP. For systems with solid sorbents, the sorption process can be physical (using materials like activated carbon, silica gel, zeolite), or chemical (using salts or metal hydrides). The most important practical differences between physical and chemical adsorption are: (i) the former is divariant and the latter is monovariant; and (ii) the former occurs almost instantaneously when the adsorbent is put in contact with the gas, if there is no severe problem of mass transfer, while in the latter, the velocity of the reaction depends on how far the temperature or pressure are from the salt equilibrium.

According to Dubinin [1], the thermodynamical equilibrium of physical adsorption in meso or macropores can be expressed by equations like BET or Langmuir because the adsorbate forms mono or multi-layers on the surface of the solid. These equations cannot be employed for physical adsorption in micropores because the adsorption occurs not in layers but in the whole volume of the pores, and according to Huber et al. [2], the equation of Dubinin–Astakhov is more appropriate. Passos [3], Tamainot-Telto and Critoph [4], Wang [5] and Oliveira et al. [6] have identified the coefficients of the Dubinin–Astakhov equation for activated carbon, which is the most studied physical adsorbent for ice making, with different adsorbates, including ammonia and methanol.

To assess the conditions in which the chemisorption occurs, it is important to identify the thermodynamic equilibrium of the reaction, which is related to its enthalpy and entropy, and also the kinetics coefficients related to the velocity of the reaction. Neveu and Castaing [7] showed several values of enthalpy and entropy, collected from the literature, for reactions involving chlorides and ammonia, and different approaches can be used to identify the kinetics coefficients depending on how the authors decide to describe the reaction and perform their experiments.

The kinetics coefficients for the pair $SrCl_2$–NH_3 were identified by Huang et al. [8], while Lu et al. [9] and Han et al. [10] identified them for the pair $MnCl_2$–NH_3. Lebrun and Spinner

* Corresponding author. Tel.: +86 21 34204263; fax: +86 21 34206814.
E-mail address: baxihujie@sjtu.edu.cn (R.G. Oliveira).

1385-8947/$ – see front matter © 2007 Elsevier B.V. All rights reserved.
doi:10.1016/j.cej.2007.06.019

Nomenclature

A_{Ev}	cross-section area of the evaporator (m^2)
K	kinetic coefficient (s^{-1})
Cp	specific heat ($J\,°C^{-1}\,kg^{-1}$)
$\hat{C}p$	molar specific heat ($J\,°C^{-1}\,mol^{-1}$)
h	liquid level inside the evaporator during the synthesis reaction (m)
h_0	liquid level inside the evaporator at the beginning of the synthesis reaction (m)
H_l	enthalpy of liquid refrigerant ($J\,kg^{-1}$)
ΔH_S	reaction heat ($J\,mol^{-1}$)
H_{vl}	gas–liquid phase change enthalpy ($J\,kg^{-1}$)
I_0	source term ($mol\,m^{-3}$)
m_{ad}	ammonia absorbed per mass unit of salt ($kg\,kg^{-1}$)
m_S	mass of salt (kg)
m, n	kinetics coefficient
Δm_{ad}	variation of absorbed ammonia per mass unit of salt (kg kg)
M	molar mass ($kg\,kmol^{-1}$)
P	pressure (bar, Pa)
P_{Eq}	equilibrium pressure (Pa)
r	radius (m)
R	gas constant ($J\,kmol^{-1}\,K^{-1}$, $J\,mol^{-1}\,K^{-1}$)
SCP	specific cooling power ($W\,kg^{-1}$)
t	synthesis time (s)
T	temperature (K, °C)
T_{Eq}	equilibrium temperature (K)
U	overall heat transfer coefficient ($W\,°C^{-1}\,m^{-2}$)
V	volume (cm^3, m^3)
V_R	void volume of the reactor (m^3)
X	global conversion

Greek letters

γ	stoichiometric coefficient ($mol\,mol^{-1}$)
ε	porosity
κ	apparent bed permeability (m^2)
λ	apparent thermal conductivity ($W\,m^{-1}\,°C^{-1}$)
μ	gas viscosity ($kg\,m^{-1}\,s^{-1}$)
ν	molar volume ($m^3\,mol^{-1}$)
ρ	density ($kg\,m^{-3}$)
$\hat{\rho}_{SB}$	molar density of the salt in the block ($mol\,m^{-3}$)

Subscripts

0.90	90% of global conversion
24	conversion of $CaCl_2{\cdot}2NH_3$ into $CaCl_2{\cdot}4NH_3$
48	conversion of $CaCl_2{\cdot}4NH_3$ into $CaCl_2{\cdot}8NH_3$
B	block
Ch	gas channel
Cn	condensation
EG.B	expanded graphite in the block
Ev	evaporation
G	gas
Gr	graphite
HTF	heat transfer fluid
Max	maximum
Out	outer side
S	salt
S2	salt with two moles of ammonia
S4	salt with four moles of ammonia
S8	salt with eight moles of ammonia
W	wall

[11], Mazet et al. [12], and Goetz and Marty [13] identified the coefficients for the two reactions involved when the CH_3NH_2 reacts with $CaCl_2$.

In the study performed by Iloeje et al. [14], the authors used coefficients for the pair $CaCl_2$–NH_3, which were obtained by correlation with the data for the pair $SrCl_2$–NH_3. These authors also assumed that the kinetics in the synthesis and decomposition could be described by equations with the same coefficients, which is not in agreement with other studies [8,9].

Hosatte-Ducassy and Rheault [15] experimentally studied the synthesis and decomposition of $CaCl_2{\cdot}8NH_3$ and $CaCl_2{\cdot}4NH_3$, separately. However, when $CaCl_2$ and NH_3 are used in refrigeration systems, the synthesis of $CaCl_2{\cdot}8NH_3$ and $CaCl_2{\cdot}4NH_3$ can occur simultaneously, and the authors did not give any indication of how to treat these two reactions simultaneously or if the identified coefficients could be employed in this situation.

In the present work the kinetics coefficients for the reactions involving the pair $CaCl_2$–NH_3 were identified when the synthesis of $CaCl_2{\cdot}8NH_3$ and $CaCl_2{\cdot}4NH_3$ occurs simultaneously. In addition to the kinetics coefficients, the heat transfer and mass transfer coefficients of the reactive bed were also identified. The bed is similar to the bed studied by Oliveira et al. [16], which is promising for use is sorption icemakers. The cooling power per mass of reactive salt can be more than 1000 W in the range of evaporation temperature from −10 to −20 °C, if the heat sink has temperatures of between 20 and 30 °C.

2. Experimental procedures

The coefficients for the kinetics, mass transfer and heat transfer models were identified by minimizing the sum of the squared deviations between the experimental and simulated data.

The experiments were performed in the test rig shown in Fig. 1a, which was filled with two 113 g blocks of consolidated composite sorbent.

The blocks were made of expanded graphite powder, which was previously immersed in a 14% $CaCl_2$ solution and dried until all the water was removed, as described previously by Oliveira et al. [16]. The powder with 50% $CaCl_2$ and 50% expanded graphite was then inserted in a mold and compressed with a pressure of 10 MPa for approximately 30 s. The final bulk density was 0.58 $g\,cm^{-3}$.

The sensible and reaction heats from the reactive blocks were removed by a heat sink, which the temperature was set to 20, 25

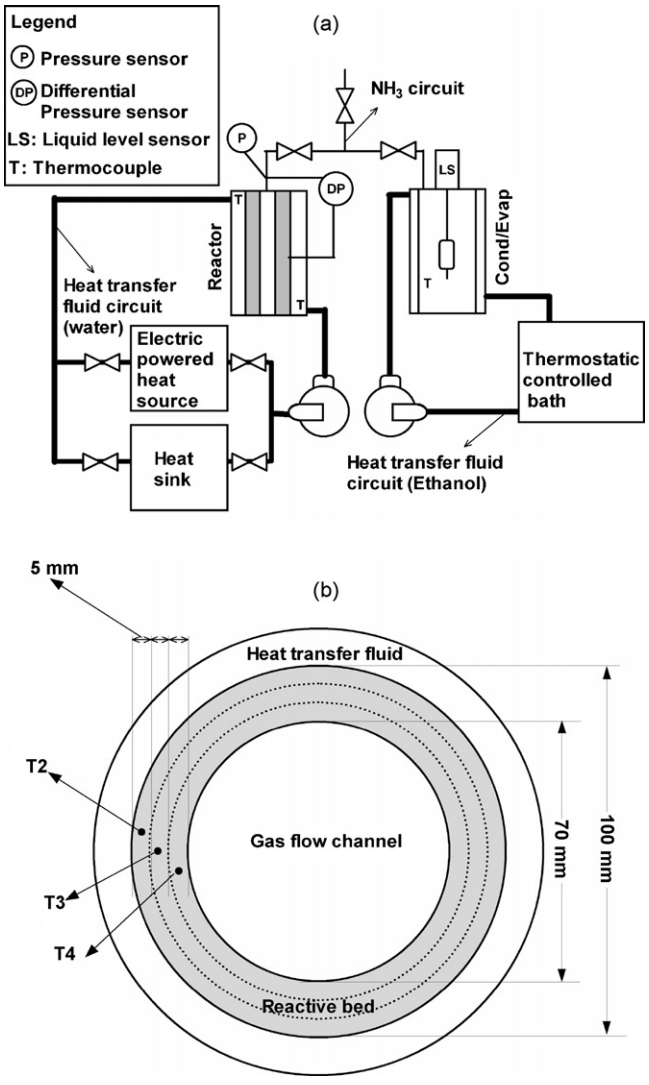

Fig. 1. (a) Experimental test rig; (b) position of the temperature sensors.

and 30 °C. The evaporation pressure ranged from 1.74 ± 0.16 to 2.95 ± 0.38 bar. Although the heat sink temperature could be kept reasonably constant (standard deviation smaller than 0.3 °C), the evaporation pressure changed greatly during the reactions, with the standard deviation being more than 10% of the mean value.

In each experiment, the initial temperature difference between the bed and the heat sink was less than 1 °C, and the ammonia in the evaporator had a constant temperature equal to the set-point temperature (−5, −15 and −20 °C). The valve between the reactor and the evaporator was then opened, the ammonia flowed from one vessel to the other, and the synthesis reactions started to occur.

The bed was 15 mm thick and the temperature was measured at three radial positions, according to the Fig. 1b. The pressure was measured at the gas channel, and a differential pressure sensor measured the difference between the pressure close to the wall and at the gas channel. A magnetostrictive sensor was used to assess the variation of the ammonia level in the evaporator. The absorbed mass per mass of salt was calculated using Eq. (1), and the global conversion was calculated with Eq. (2).

$$m_{ad} = \frac{-[(h - h_0)A_{Ev}\rho_{NH_3} + (M_{NH_3}V_R/RT_G)(dP/dt)]}{m_S} \quad (1)$$

$$X = \frac{m_{ad}}{m_{ad.Max}} \quad (2)$$

The temperature of the ammonia vapour (T_G) was assumed to be similar to the temperature in the portion of the bed close to the inlet/outlet gas channel.

A set of equations was codified in the software SCIENTIST (Micromath, Salt Lake City, UT, USA) to simulate both the variation of temperature and pressure of the bed, and the evolution of the reactions shown in Eqs. (3) and (4):

$$CaCl_2{\cdot}2NH_3 + 2NH_3 \Leftrightarrow CaCl_2{\cdot}4NH_3 + 2\Delta H_{24} \quad (3)$$

$$CaCl_2{\cdot}4NH_3 + 4NH_3 \Leftrightarrow CaCl_2{\cdot}8NH_3 + 4\Delta H_{48} \quad (4)$$

The software employs a stiff EPISODE integrator and a modified Powell algorithm to find a local or global minimum of the sum of the squared deviations between the observed and calculated data. The kinetics, heat transfer and mass transfer equations used in the simulation are shown in the next subsections.

According to Lebrun and Spinner [11], the kinetics models can be phenomenological or analogical, each having its advantages and disadvantages. The phenomenological models, although more precise for a large range of conditions, require a deeper understand of the structure and properties of the reacting medium and may be cumbersome to manipulate, leading to a large simulation time. The analogical models consider all the phenomena that might affect the reaction kinetic in a global way. Instead of a detailed description of the mechanisms involved in the reaction, the analogical model aims to reproduce the overall effect. Moreover, the model does not describe the reactive medium at the particulate level, where different materials are treated as separate entities, but rather assumes the existence of an equivalent single material, which is a combination of the other materials. Therefore, the analogical model can describe the differences in temperature and pressure at different portions of the reactive bed at a certain time, but not the differences that might occur in the different materials.

The analogical model was chosen in this work due to the limited information about the granulometric repartition, porosity, and inter and intra granular diffusivity of the bed composed of compressed expanded graphite impregnated with $CaCl_2$.

Due to the fact that this kind of model is only valid in conditions similar or close to the studied ones, the experiments were performed under several temperatures and pressures normally employed in sorption icemakers, to validate the model over a useful range of operation conditions.

2.1. Description of the kinetics

The kinetics of the reaction with salts at constant pressure are usually described as a function of equilibrium drop (ΔEQ equal to ΔP_{Eq} or ΔT_{Eq} in Fig. 2), the Arrhenius factor (Ar) and the vacant sites for reaction ($f(X)$), in a generic form presented

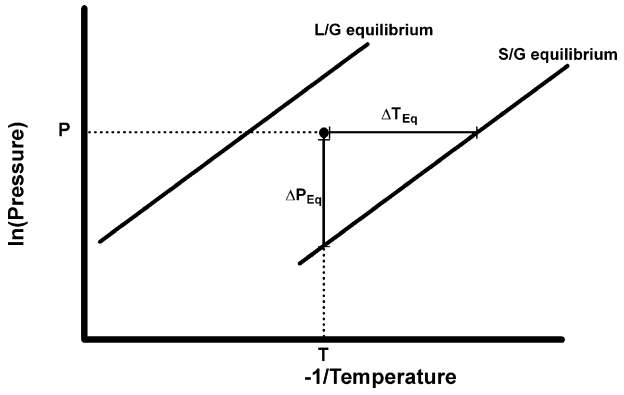

Fig. 2. Clapeyron diagram.

in Eq. (5).

$$\frac{dX}{dt} = f(X)\mathrm{Ar}\,\Delta\mathrm{EQ} \tag{5}$$

Assuming that the reaction occurs in a homogeneous medium, the vacant sites can be represented as:

$$f(X) = (1 - X)^n \tag{6}$$

where X is the degree of conversion in the reaction, which ranges from zero to one, and n is related to how the vacant sites influence the reaction.

In this study, two reactions could occur together, and the production of $CaCl_2{\cdot}8NH_3$ did not occur before the production of $CaCl_2{\cdot}4NH_3$; thus, the vacant sites of the second reaction were described by:

$$f(X_{48}) = (X_{24} - X_{48})^n \tag{7}$$

The subscripts 24 and 48 are related to the reactions shown in Eqs. (3) and (4), respectively.

The Arrhenius factor is indicative of how the velocity of the reaction changes with temperature. However, according to some authors [10,12], this parameter is almost constant in the range of operating conditions normally employed for a heat pump or refrigeration chemisorption machine, and thus, it was considered as a constant coefficient (K) in the presented model.

The deviation from the equilibrium can be written in different forms [11,12,14]. In the presented model, a quadratic approach was used. It considers equilibrium drops related to both temperature and pressure, as shown in Eq. (8).

$$\Delta\mathrm{EQ} = \ln\left(\frac{P}{P_{\mathrm{Eq}}}\right)\left(\frac{1}{T_{\mathrm{Eq}}} - \frac{1}{T}\right) \tag{8}$$

Eq. (8) was used instead of the linear equilibrium drops proposed in references [11,12,14], because it produced better fit between the experimental and simulated data. The reason for this better fit is not fully understood, but it could be related to the fact that there is a zone near equilibrium where no or almost no reaction occurs, as mentioned by some authors [17,18]. Then, due to the existence of this non-reaction zone (which is larger at lower pressures), the velocity of the reaction may increase at a rate that is better describer when both the temperature and pressure equilibrium drops are taken into account.

It can be noted in Eq. (5) that there is no term related to the pressure in which the reaction occurs. The number of particles of gas around the particles of salt is proportional to the pressure of the system; thus, it is reasonable to assume that for the same equilibrium drop, higher pressure would increase the reaction rate because the number of particles available to react in a fixed volume would also increase. Therefore, assuming the refrigerant in the gas phase as an ideal gas, the number of moles of refrigerant in the void space of the bed per mol of salt (N) can be calculated by Eq. (9):

$$N = \left(\frac{P\varepsilon}{RT\hat{\rho}_{\mathrm{SB}}}\right)^m \tag{9}$$

The empirical exponential term m is indicative of how the influence of the gas molecules in the void space changes with its concentration, and improves the fit between the experimental and simulated data.

The combination of Eqs. (5)–(9) results in Eqs. (10) and (11), which were used to calculate the conversion rate for the synthesis of $CaCl_2{\cdot}8NH_3$ from $CaCl_2{\cdot}4NH_3$ and $CaCl_2{\cdot}2NH_3$.

$$\frac{dX_{24}}{dt} = K_{24}(1 - X_{24})^{n24}\left(\frac{P\varepsilon}{RT\hat{\rho}_{\mathrm{SB}}}\right)^{m24} \times \ln\left(\frac{P}{P_{\mathrm{Eq24}}}\right)\left(\frac{1}{T} - \frac{1}{T_{\mathrm{Eq24}}}\right) \tag{10}$$

$$\frac{dX_{48}}{dt} = K_{48}(X_{24} - X_{48})^{n48}\left(\frac{P\varepsilon}{RT\hat{\rho}_{\mathrm{SB}}}\right)^{m48} \times \ln\left(\frac{P}{P_{\mathrm{Eq48}}}\right)\left(\frac{1}{T} - \frac{1}{T_{\mathrm{Eq48}}}\right) \tag{11}$$

The global conversion rate (X) for the reactions shown in Eqs. (3) and (4) was calculated using Eq. (12), which considers the contribution of each reaction to the total absorbed ammonia:

$$\frac{dX}{dt} = \frac{\sum_{i=1}^{3} V_i[\{4(dX_{48}/dt) + 2(dX_{24}/dt)\}/6]_i}{V_{\mathrm{B}}} \tag{12}$$

The subscript i refers to each imaginary layer instrumented with a thermocouple, as shown in Fig. 1b. The temperatures T_i acquired by the thermocouples during the reactions were used in the above equations. For the layer near the gas channel, the pressure P was assumed to be the pressure read by the pressure sensor. The pressure in the layer near the wall was assumed to be the difference between the values measured by the pressure and differential pressure sensors. The pressure in the middle layer was assumed to be an arithmetic average of the pressure in the other two layers. The temperature and pressure inside each layer was assumed uniform. The velocity of the reaction was obtained with Eq. (2), in the range of global conversion from 0 to 0.92; therefore, the only unknown constants in Eqs. (10) and (11) were the three kinetics coefficients for each reaction.

The identified kinetics coefficients for each experimental condition were those that minimize the sum of the squared deviations between the observed and the calculated data. The final value for each coefficient was the arithmetic average of the values obtained under each experimental condition.

2.2. Heat transfer model

It was assumed that the heat within the bed was only transferred by conduction in the radial direction, and the convective heat of the gas was neglected. The heat transfer equation (Eq. (13)) was discretized in three control volumes, analogous to the imaginary layers of the reactive block that were instrumented with thermocouples, as shown in Fig. 1b. The temperatures measured by these sensors were inserted in Eq. (13), the conversion in each layer was calculated with Eqs. (10) and (11), and the only unknown parameters were those related to the apparent thermal conductivity of the bed and the overall heat transfer coefficient, which appear in the boundary condition. The thermal coefficients λ_1, λ_2, U_1 and U_2 in Eqs. (16) and (17) were assessed simultaneously in each experimental condition. Similar to the procedure adopted in identification of the kinetics coefficients, the final value of each thermal coefficient was the average of the values obtained under the different operation conditions.

$$\left(\sum_{i=1}^{3}\rho Cp\right)\frac{\partial T}{\partial t} = \lambda\frac{\partial}{r\partial r}\left(r\frac{\partial T}{\partial r}\right) + \hat{\rho}_{SB}\left[\left(\gamma\Delta H_S\frac{\partial X}{\partial t}\right)_{24} + \left(\gamma\Delta H_S\frac{\partial X}{\partial t}\right)_{48}\right] \quad (13)$$

The boundary conditions are:

$$\text{At } r = r_W, \quad -\lambda\frac{\partial T}{\partial r} = U(T_{HTF} - T) \quad \forall t \quad (14)$$

$$\text{At } r = r_{Ch}, \quad -\lambda\frac{\partial T}{\partial r} = 0 \quad \forall t \quad (15)$$

The overall heat transfer coefficient (U) was assumed to be a linear function of the global conversion in the layer closer to the wall (Eq. (16)), and the apparent thermal conductivity was assumed to be a linear function of the global conversion (Eq. (17)).

$$U = U_1 X_W + U_2 \quad (16)$$

$$\lambda = \lambda_1 X + \lambda_2 \quad (17)$$

The volumetric heat capacity of the block $\left(\sum_{i=1}^{3}(\rho Cp)_i\right)$ was calculated with Eq. (18), and considering the contributions of the expanded graphite, the gas and the different ammoniates that may exist simultaneously.

$$\sum_{i=1}^{3}(\rho C)_i = (\rho Cp)_{EG.B} + \hat{\rho}_{SB}[(\hat{C}p_{S8} - \hat{C}p_{S4})X_{48} + (\hat{C}p_{S4} - \hat{C}p_{S2})X_{24} + \hat{C}p_{S2}] + \rho_{NH_3}\varepsilon \quad (18)$$

The porosity of the bed (ε) was calculated with Eq. (19a), which is similar to the form proposed by Han and Lee [19].

$$\varepsilon = 1 - \frac{V_{Gr}}{V_B} - \frac{V_S}{V_B} \quad (19a)$$

$$\varepsilon = 1 - \frac{\rho_{EG.B}}{\rho_{Gr}} - \left[\frac{(1-f_g)}{f_g}\right][\upsilon_{S2} + (\upsilon_{S4} - \upsilon_{S2})X_{24} + (\upsilon_{S8} - \upsilon_{S4})X_{48}]\frac{\rho_{EG.B}}{M_S} \quad (19b)$$

The mass fraction of expanded graphite in the block (f_g) was 0.5. The specific heat for the ammoniates (Cp_{S8}, Cp_{S4} and Cp_{S2}) were those presented by Hosatte-Ducassy and Rheault [15]. The density of the expanded graphite in the blocks ($\rho_{EG.B}$) was half of the apparent bulk density, and values for molar volume of the ammoniates (ν_{S8}, ν_{S4} and ν_{S2}) were taken from Han and Lee [19].

2.3. Mass transfer model

Assuming that the gas flows only in the radial direction and that the mass of gas is consumed according to the velocity of the reaction, the equation of one-dimensional mass transfer can be expressed as:

$$\varepsilon\frac{\partial P}{\partial t} = \varepsilon\frac{P}{T}\left(\frac{\partial T}{\partial t}\right) + \frac{RT}{r}\frac{\partial}{\partial r}\left(r\frac{D}{RT}\frac{\partial P}{\partial r}\right) - RTI_0 \quad (20)$$

The source term (I_0) is related to the consumption of gas and it was calculated with Eq. (21). The diffusivity (D) was calculated according to Darcy's Law, as shown in the Eq. (22):

$$I_0 = \hat{\rho}_{S.B}\left[\left(\gamma\frac{\partial X}{\partial t}\right)_{24} + \left(\gamma\frac{\partial X}{\partial t}\right)_{48}\right] \quad (21)$$

$$D = \frac{\kappa P}{\mu} \quad (22)$$

The values for the temperatures T used in the mass transfer model were those obtained by the heat transfer model, and the velocity of the reaction was obtained with the kinetic model. The boundary conditions were:

$$\text{At } r = r_W, \quad \frac{\partial P}{\partial r} = 0 \quad \forall t \quad (23)$$

$$\text{At } r = r_{Ch}, \quad P = P_{Ev} \quad \forall t \quad (24)$$

The only unknown constants were the coefficients related to the apparent permeability of the bed (κ), which was assumed to increase linearly with the porosity of the bed (ε), as shown in Eq. (25):

$$\kappa(\varepsilon) = \kappa_1\varepsilon - \kappa_2 \quad (25)$$

3. Results and discussion

3.1. Identification of the coefficients for the models

To identify the kinetics coefficients, m_{24} and m_{48} were first assumed equal to one. The results showed that the best fit for the different operation conditions was obtained when n_{24} was close to 2 and n_{48} was close to 1. The substitution of the value of the coefficients m from one to two produced similar results. Then, the coefficients n were rounded to the closest integer value, and for the subsequent fits the n_{24} was equal to two and n_{48} equal to

Table 1
Kinetics coefficients

K_{24} (s^{-1})	1.120e5
n_{24}	2
m_{24}	2
K_{48} (s^{-1})	1.025e4
n_{48}	1
m_{48}	1

one. New fits were performed with n fixed, while m and K varied. The coefficients m showed to be very sensitive to the initial conditions used in the fitting, and the results greatly changed according to the initial values assumed for these coefficients. Thus, the pair m_{24}–m_{48} received fixed values equal to 1–1, 1–2, 2–1 and 2–2, and only the value of K had to be identified. For each of these pairs of values, K slighted changed according to the experimental condition. As the purpose of the experiments was to identify coefficients that could describe the reactions in all the studied conditions, the values of m_{24} equal to 2 and m_{48} equal to 1 were chosen because they resulted in the smallest relative deviation between the K obtained in each experimental condition. The final values for K_{24} and K_{48} were, respectively, the average values of the K_{24} and K_{48} obtained in each experimental condition.

The kinetics coefficients are shown in Table 1, the average absolute error at each experimental condition is shown in Table 2, and Fig. 3 shows the experimental and simulated data with the coefficients identified for the kinetics, heat transfer and mass transfer models.

The average relative error among all the conditions studied was $2.4 \pm 1.4\%$ when the global conversion was 0.90, and the maximum value was 4.6% under a heat sink temperature of 25 °C and an evaporation pressure of 2.51 bar. However, when the influence of the pressure was not taken into account in the kinetic model, and the equilibrium drop was described in the form of $\ln P/P_{Eq}$ as suggested by Lebrum and Spinner [11], the average relative error was $4.4 \pm 2.9\%$. In this case, the average absolute error at the experimental condition T_{HTF} of 30 °C and P_{Ev} of 1.74 bar could be as high as 0.117 ± 0.73, instead of 0.021 ± 0.016, as shown in Table 2.

Although the assumptions that the overall heat transfer coefficient and apparent thermal conductivity vary linearly with the global conversion and that the apparent permeability varies linearly with the porosity of the bed may seem far-fetched, the identified coefficients shown in Table 3 produced a good fit to the experimental data as can be seen in Figs. 4 and 5.

Table 2
Global conversion errors at different heat sink temperatures and evaporation pressures

P_{Ev} (bar)	T_{HTF} (°C)	Error
2.61 ± 0.46	20	0.024 ± 0.016
2.51 ± 0.37	25	0.041 ± 0.015
2.95 ± 0.38	30	0.026 ± 0.018
1.90 ± 0.27	20	0.023 ± 0.017
2.05 ± 0.25	25	0.030 ± 0.017
2.02 ± 0.19	30	0.012 ± 0.011
1.75 ± 0.19	25	0.020 ± 0.009
1.74 ± 0.16	30	0.021 ± 0.016

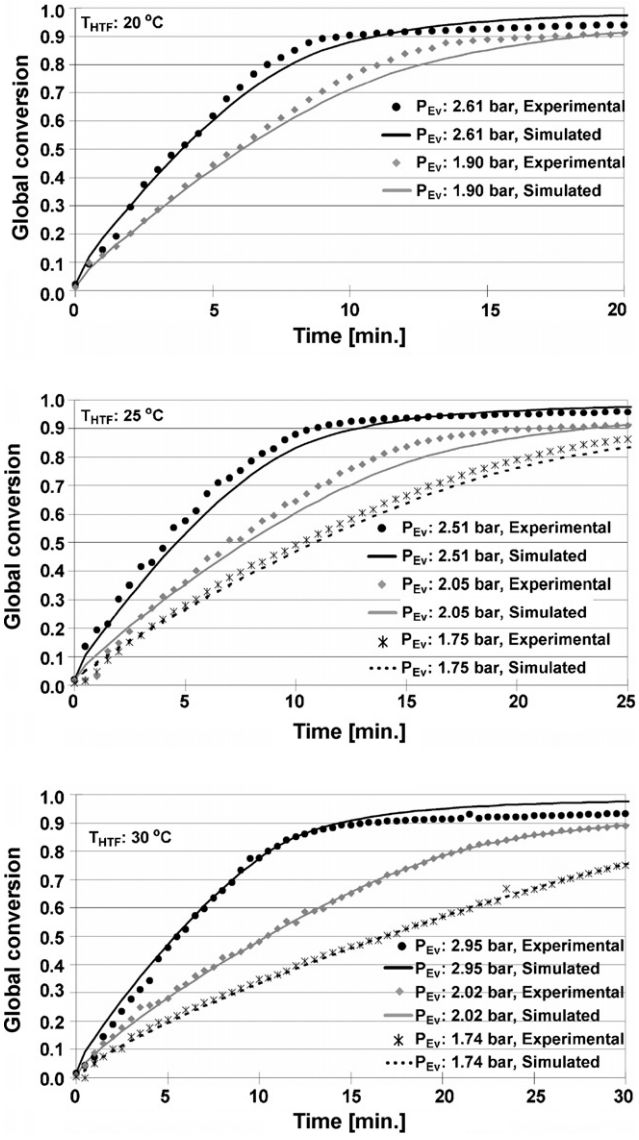

Fig. 3. Global conversion under different experimental conditions.

The average error between the measured and simulated temperature was no more than 1.3 °C, under any experimental condition. The maximum error ranged from 1.8 to 4.0 °C according to the experimental condition, and always occurred at the beginning of the reaction for the temperature simulated in the layer closer to the gas channel.

From the coefficients assessed for the heat transfer model it is possible to note that the overall heat transfer coefficient

Table 3
Coefficients for the heat and mass transfer models

U_1 ($W m^{-2} °C^{-1}$)	285
U_2 ($W m^{-2} °C^{-1}$)	747
λ_1 ($W m^{-1} °C^{-1}$)	4.25
λ_2 ($W m^{-1} °C^{-1}$)	7.41
κ_1 (m^2)	9.22e−14
κ_2 (m^2)	2.59e−14

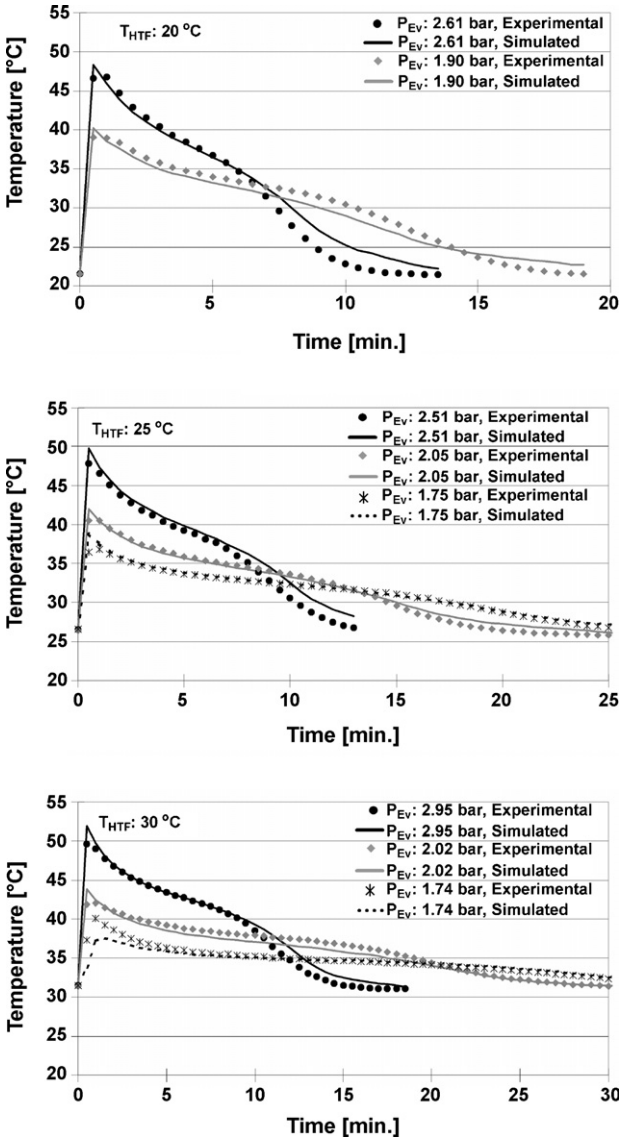

Fig. 4. Average temperature of the bed under different experimental conditions.

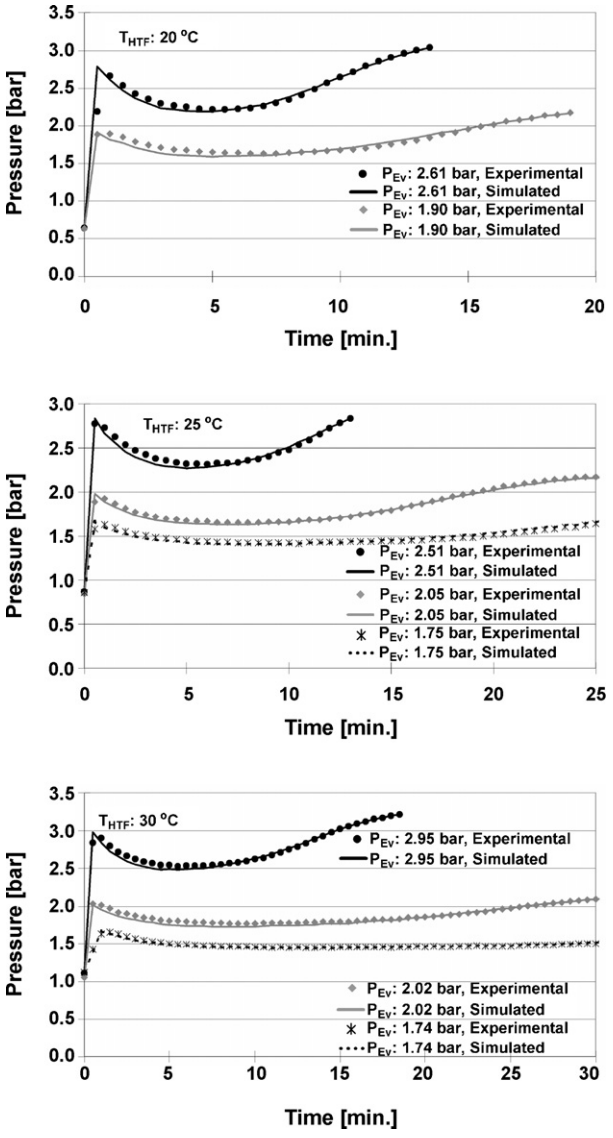

Fig. 5. Pressure close to the wall under different experimental conditions.

between the reactive bed and the coolant increased 38%, and the apparent thermal conductivity increased 57% when the ammoniate in the form $CaCl_2.2NH_3$ was converted into $CaCl_2{\cdot}8NH_3$. The assessed apparent thermal conductivity of the bed was 7.41 W m^{-1} °C^{-1} when the salt had two moles of ammonia absorbed and 11.66 W m^{-1} °C^{-1} for eight moles.

The simulation of the pressure close to the wall of the reactor produced average errors in the range of 12–47 mbar, according to the experimental condition. The maximum error, in any condition, was between 44 and 593 mbar and always occurred in the first minute of synthesis. The apparent bed permeability varied from 3.59×10^{-14} to 9.96×10^{-15} m^2 during the conversion of $CaCl_2{\cdot}2NH_3$ into $CaCl_2{\cdot}8NH_3$.

3.2. Simulation of reactive beds with different dimensions

In order to assess the expected specific cooling power (SCP) of a sorption icemaker using the studied reactive compound, two configurations were simulated where the inner diameter was kept constant at 20 mm and the outer diameter was 40 or 60 mm. The heat sink temperatures were 20, 25 or 30 °C, and the evaporation pressures were 1.90, 2.36 or 2.91 bar, which correspond to evaporation temperatures of −20, −15 and −10 °C, respectively. At each condition, two positions for the heat sink were assumed: (1) outer side, with refrigerant mass flow from the inner side; (2) inner side, with refrigerant mass flow from the outer side. The SCP was calculated according to Eq. (26), assuming 90% conversion.

$$\mathrm{SCP} = [H_{\mathrm{vl}}(T_{\mathrm{Ev}}) - (H_{\mathrm{l}}(T_{\mathrm{Cn}}) - H_{\mathrm{l}}(T_{\mathrm{Ev}}))]\frac{\Delta m_{\mathrm{ad\_0.90}}}{\Delta t_{0.90}} \qquad (26)$$

It is possible to see in Figs. 6 and 7 that the SCP obtained at better reaction conditions (higher pressures, lower heat sink temperatures) can be about four to five times the value obtained under the worse conditions. As the heat sink temperature is usually limited by the ambient temperature, in situations where it cannot be lower than 30 °C, the reactions should be carried out under

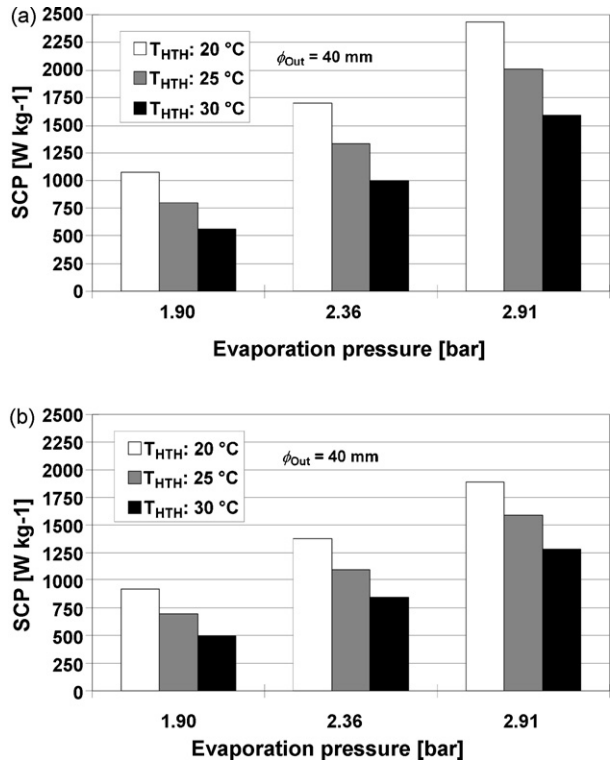

Fig. 6. SCP under different simulated conditions. Ten millimeters thickness bed: (a) heat sink position 1; (b) heat sink position 2.

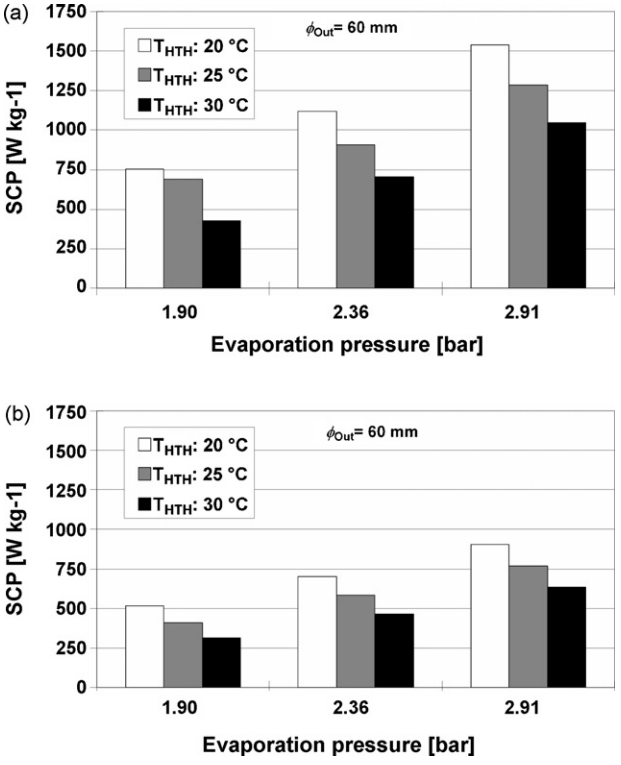

Fig. 7. SCP under different simulated conditions. Twenty millimeters thickness bed: (a) heat sink position 1; (b) heat sink position 2.

the highest possible evaporation temperatures to ensure relative high SCP. Temperatures of −10 °C are suitable to be employed in ice production, and if an evaporator with good heat transfer properties is used, the evaporation temperature can be kept closer to the ice temperature, and the evaporation pressure can be kept at the highest possible value, leading to a higher SCP.

The thickness of the bed also has a great influence on the SCP, and it become even more important when the heat sink is placed in the inner part of the bed, which has the smallest relation between the heat transfer area and the block volume. When the heat sink is in the outer side of the reactor, the SCP of the bed 10 mm thick can be 31 to 58% higher than that of the bed 20 mm thick, with the biggest differences occurring for operation conditions more favourable for the reaction. If the heat sink is moved to the inner side, which is the most common situation, the difference of the SCP can be on the order of 60–109%.

4. Conclusion

From the presented results, it is possible to conclude that the analogical model with the identified coefficients is suitable to simulate the synthesis of $CaCl_2{\cdot}8NH_3$ from $CaCl_2{\cdot}2NH_3$ when $CaCl_2{\cdot}8NH_3$ and $CaCl_2{\cdot}4NH_3$ are produced simultaneously in an expanded graphite matrix bed. The introduction of the pressure influence in the model allowed using the same coefficients to simulate the reaction under the range of evaporation pressures normally employed in sorption icemakers, and in non-isobaric conditions.

The assumption that the overall heat transfer coefficient and the apparent thermal conductivity vary linearly with the global conversion, and that the apparent permeability varies with the porosity of the bed were shown to be suitable for use in simulations of reactors using the studied consolidated compound under different designs, e.g. smaller or large thickness, or different working conditions.

The identified apparent thermal conductivity for the reactive blocks ranged from 7.41 to 11.66 $W\,m^{-1}\,°C^{-1}$, and the overall heat transfer coefficient was on the order of 747 to 1032 $W\,m^{-2}\,°C^{-1}$, according to the degree of reaction. The maximum error of the simulated temperature was no more than 4.0 °C, and the average error was 1.3 °C or below, under any studied condition. The apparent permeability of the bed varied between 3.59×10^{-14} and $9.96 \times 10^{-15}\,m^2$, and the average error of the pressure close to the reactor wall calculated by simulations was smaller than 50 mbar.

The results of the simulation demonstrate the importance of the equilibrium drop and the bed thickness to obtain high SCP. For example, when a bed 10 mm thick is cooled by a heat sink at 25 °C, synthesis could be carried out at evaporation temperatures of −15 °C with SCP higher than 1250 $W\,kg^{-1}$. However, in a bed of 20 mm thickness, SCP above 1250 $W\,kg^{-1}$ can only be obtained if the evaporation temperature is at least −10 °C.

Acknowledgements

This work was supported by National Science Fund for Distinguished Young Scholars of China under the contract No.

50225621, Shanghai Shuguang Training Program for the Talents under the contract No. 02GG03.

References

[1] M.M. Dubinin, Adsorption in micropores, J. Colloid Interface Sci. 23 (1967) 487.
[2] U. Huber, F. Stoeckli, J.P.A. Houriet, Generalization of the Dubinin-Radushkevich equation for the filing of heterogeneous micropore systems in strongly activated carbons, J. Colloid Interface Sci. 67 (1978) 195.
[3] F.P. Passos, Etude des couples charbon actif/methanol et de leur application a la refrigerations solaire. Ecole Polytechnique Federale de Lausanne [Ph.D.] (1986) 1.
[4] Z. Tamainot-Telto, R.E. Critoph, Adsorption refrigerator using monolithic carbon-ammonia pair, Int. J. Refrig. 20 (1997) 146.
[5] R.Z. Wang, Adsorption refrigeration research in Shanghai Jiao Tong University, Renew. Sust. Energ. Rev. 5 (2001) 1.
[6] R.G. Oliveira, Z. TamainotTelto, V. Silveira Jr., Equilibrium characterisation of carbon C119-ammonia and carbon C119-dimethyl ether pairs and application in adsorption refrigeration design, in: Proceedings of COBEM, Brazil, 2001.
[7] P. Neveu, J. Castaing, Solid-gas chemical heat pumps: field of application and performance of the internal heat of reaction recovery process, Heat Recov. Syst. CHP 13 (1993) 233.
[8] H.J. Huang, G.B. Wu, J. Yang, Y.C. Dai, W.K. Yuan, H.B. Lu, Modeling of gas-solid chemisorption in chemical heat pumps, Sep. Purif. Technol. 34 (2004) 191.
[9] H.B. Lu, N. Mazet, B. Spinner, Modelling of gas-solid reaction-coupling of heat and mass transfer with chemical reaction, Chem. Eng. Sci. 51 (1996) 3829.
[10] J.H. Han, K.H. Lee, D.H. Kim, H. Kim, Transformation analysis of thermochemical reactor based on thermophysical properties of graphite-MnCl2 complex, Ind. Eng. Chem. Res. 39 (2000) 4127.
[11] M. Lebrun, B. Spinner, Models of heat and mass transfers in solid-gas reactors used as chemical heat pumps, Chem. Eng. Sci. 45 (1990) 1743.
[12] N. Mazet, M. Amouroux, B. Spinner, Analysis and experimental study of the transformation of a non-isothermal solid/gas reacting medium, Chem. Eng. Commun. 99 (1991) 155.
[13] V. Goetz, A. Marty, A model for reversible solid-gas reactors submitted to temperature and pressure constraints: simulation of the rate of reaction in solid-gas reactor used as chemical heat pump, Chem. Eng. Sci. 47 (1993) 4445.
[14] O.C. Iloeje, A.N. Ndili, S.O. Enibe, Computer simulation of $CaCl_2$ solid-adsorption solar refrigerator, Energy 20 (1995) 1141.
[15] S. Hosatte-Ducassy, F. Rheault, Kinetics and modelling of $CaCl_2$-NH_3 reactions, in: Proceedings of Symposium of Solid Sorption Refrigeration, 1992, p. 245.
[16] R.G. Oliveira, R.Z. Wang, C. Wang, Evaluation of the cooling performance of a consolidated expanded graphite-calcium chloride reactive bed for chemisorption icemaker, Int. J. Refrig. 30 (2007) 103.
[17] E. Lepinasse, B. Spinner, Production de froid par couplage de réacteurs solide-gaz II: Performance d'un pilote de 1 à 2 kW: Cold production through coupling of solid-gas reactors II: Performance of a pilot installation of 1 to 2 kW, Int. J. Refrig. 17 (1994) 323.
[18] N. Mazet, B. Spinner, Analyses des irréversibilités et de la problématique de recherche et développement des transformateurs thermochimiques à réaction solide-gaz: Analyses of irreversibilities and research and development on solid-gas reaction thermochemical transformers, Int. J. Refrig. 17 (1994) 329.
[19] J.H. Han, K.H. Lee, Gas permeability of expanded graphite-metallic salt composite, Appl. Therm. Eng. 21 (2001) 453.